Title

Closure for a plane fin heat sink with scale-roughened surfaces for volume averaging theory (VAT) based modeling

Journal

International Journal of Heat and Mass Transfer, 55(25-26)

ISSN

00179310

Authors

Zhou, Feng
DeMoulin, George W
Geb, David J
et al.

Publication Date

2012-12-01

DOI

10.1016/j.ijheatmasstransfer.2012.07.075

Peer reviewed

International Journal of Heat and Mass Transfer 55 (2012) 7677–7685

Contents lists available at SciVerse ScienceDirect

International Journal of Heat and Mass Transfer

journal homepage: www.elsevier.com/locate/ijhmt

Closure for a plane fin heat sink with scale-roughened surfaces for volume averaging theory (VAT) based modeling

Feng Zhou *, George W. DeMoulin, David J. Geb, Ivan Catton

Department of Mechanical and Aerospace Engineering, University of California, Los Angeles, CA, USA

ARTICLE INFO

Article history:
Received 7 January 2012
Received in revised form 19 July 2012
Accepted 25 July 2012
Available online 20 August 2012

Keywords:
Scale roughened surface
Heat sink
Volume averaging theory
Closure

ABSTRACT

The present paper describes an effort to obtain closure for a volume averaging theory (VAT) based model of a plane fin heat sink (PFHS) with scale-roughened surfaces by evaluating the closure terms for the model using computer fluid dynamics (CFD). Modeling a PFHS as porous media based on VAT, specific geometry can be accounted for in such a way that the details of the original structure can be replaced by their averaged counterparts and the VAT based governing equations can be efficiently solved for a wide range of parameters. To complete the VAT based model, proper closure is needed, which is related to a local friction factor and a heat transfer coefficient of a representative elementary volume (REV). The terms in the closure expressions are complex and sometimes relating experimental data to the closure terms is difficult. In this work we use CFD to obtain detailed solutions of flow and heat transfer through an element of the scale-roughened heat sink and use these results to evaluate the closure terms needed for a fast running VAT based code, which can then be used to solve the heat transfer characteristics of a higher level heat sink. The objective is to show how heat sinks can be modeled as a porous media based on volume averaging theory and how CFD can be used in place of a detailed, often formidable, experimental effort to obtain closure for a VAT based model.

1. Introduction

With the trend towards increasing levels of electronic device integration density, it has become increasingly challenging to meet the thermal management requirements of the resulting elevated power dissipation. A variety of techniques [1] for heat transfer enhancement have been developed, including ribs [2–6], pin fins [7–9], dimpled surfaces [10–12], surfaces with arrays of protrusions [13], and surface roughness. The design objective of these techniques is to significantly enhance convective heat transfer without substantially increasing in the streamwise pressure drop penalty.

A new heat transfer enhancement surface geometry was developed by Chang et al. [14–18] using deepened scale-roughened surfaces. The geometrical details of the proposed scale roughened surface are shown in Fig. 1. The surface scales are arranged in a staggered manner in-line on opposing walls. The authors compared $\overline{Nu}/Nu_\infty$ and $\bar{f}/f_\infty$ of the scale roughened surface with the flow and heat transfer results reported by different research groups for rib-roughened channels [2–6] and dimpled surfaces [10]. The heat transfer enhancement of the scale-roughened surface was surprisingly good compared with rib-roughened and dimpled surfaces and the channel with forward flow performs better than that with backward flow.

A scale-roughened surface is a promising heat transfer enhancement technique and can be applied to plane fin heat sinks to augment their heat dissipation capability, see Fig. 2, but further optimization is required. If one wants to optimize such a heat transfer device, simple equations are the only answer but they need to be made more rigorous and must include conjugate effects. In this work, VAT, see [19–30], will be used to develop the needed simple equations allowing clear rigorous statements to be made that define how the friction factor and heat transfer coefficient are to be determined. By modeling heat sinks as porous media, specific geometry can be accounted for in such a way that the details of the original structure can be replaced by their averaged counterparts and the governing VAT equations can be solved for a wide range of design parameters. This 'porous media' model, which is a function only of porous media morphology, represented by porosity and specific surface area, and its closure, can easily be adapted to many different structures.

Closure theories for transport equations in heterogeneous media have been the primary measure of advancement and for measuring success in research on transport in porous media. Obtaining

* Corresponding author. Address: Department of Mechanical and Aerospace Engineering, University of California, Los Angeles, 48-121 Engineering IV, 420 Westwood Plaza, Los Angeles, CA 90095-1597, USA. Tel.: +1 424 226 6688; fax: +1 310 206 4830.

E-mail addresses: zhoufeng@ucla.edu (F. Zhou), gdemoulin@ucla.edu (G.W. DeMoulin), geb@seas.ucla.edu (D.J. Geb), catton@ucla.edu (I. Catton).

0017-9310/$ - see front matter © 2012 Elsevier Ltd. All rights reserved.
http://dx.doi.org/10.1016/j.ijheatmasstransfer.2012.07.075

Nomenclature

A_w	wetted surface, m^2
A_{wp}	the cross flow projected area, m^2
c_p	specific heat, J/kg K
D	diameter of the scale, m
D_h	hydraulic diameter, m
d_h	hydraulic diameter defined by Chang et al. [14], m
d_p	diameter of the spherical particles, m
e	scale height, m
F_1, F_2	blending function
F_p	fin pitch, m
f	friction factor
H	channel height, m
h	heat transfer coefficient, W/m^2 K
k	turbulence kinetic energy per unit mass, m^2/s^2
k_f	thermal conductivity of the fluid, W/m K
k_s	thermal conductivity of the solid, W/m K
k_t	turbulent heat conductivity, W/m K
L	length of the channel, m
$\langle m \rangle$	porosity
Nu	Nusselt number
P_k	shear production of turbulence
Pr	Prandtl number
P_{r_t}	turbulent Prandtl number
P	scale pitch, m
p	pressure, Pa
q	heat flux, W/m^2
Re	Reynolds number
S	an invariant measure of the strain rate, 1/m
S_w	specific surface
S_{wp}	the cross flow projected area per volume, 1/m
T_s	solid temperature, K
T_f	fluid temperature, K
u_m	average velocity through the channel, m/s
W	width of the channel, m

Greeks

α	turbulence model constant or scale attack angle (°)
β, β^*	turbulence model constant
φ_1	represent any constant in the original k–ω model ($\sigma_{k1}, \cdot$)
φ_2	represent any constant in the transformed k–ε model ($\sigma_{k2}, \cdot$)
φ	represent the corresponding constant in the SST model ($\sigma_k, \cdot$)
μ	viscosity, Pa s
μ_t	turbulent eddy viscosity, Pa s
ν	kinematic viscosity, m^2/s
ν_t	turbulent kinematic viscosity, m^2/s
ρ	density, kg/m^3
σ_ε	k–ε turbulence model constant
σ_k	turbulence model constant for the k equation
σ_ω	k–ω turbulence model constant
τ_{wL}	laminar shear stress, Pa
τ_{wT}	turbulent shear stress, Pa
$\Delta\Omega$	the volume of the REV, m^3
ω	specific turbulence dissipation rate

Subscripts and superscripts

$\sim$	a value averaged over the representative volume
–	an average of turbulent values
^	fluctuation of a value
$\langle f \rangle_f$	means the superficial average of the function f
f	fluid phase
t, T	turbulent
s	solid phase

closure for the VAT based governing equation set is the most difficult aspect of using VAT to model and optimize a heat transfer device. The porosity and specific surface area are geometrically defined terms. The closure terms, which are related to a local friction factor and a heat transfer coefficient, can be obtained in two ways. The first is to rescale the available experimental data reported for fully developed flow, using the 'porous media' length scale suggested by VAT [22–24,26]. However, Chang et al. [14] only tested one specific scale-roughened surface, which is not enough to obtain the closure. At this time, CFD is an alternative approach for evaluating these closure terms [31–35]. It should be noted that if CFD is used to obtain the closure, the friction factor and heat transfer will be calculated more rigorously by integrating the complete closure formula over the REV and validated using the available experimental data.

In the following presentation, a scale-roughened plane fin heat sink with forward flow is first modelled based on volume averaging theory. 3-D numerical calculations are made to simulate the heat transfer and fluid flow across the channels which consist of 15 REVs and the CFD discretization is validated by comparison with experiment. Then, the rigorously derived closure terms are evaluated over one of the selected REVs for a range of the design parameters, and correlations for friction factor and Nusselt number are developed for use with the simple equations.

2. VAT based modeling

A schematic diagram of a plate fin heat sink with scale roughened surface is shown in Fig. 2. Generally, the air is forced to flow through the channels between the fins by a fan. The scales act to increase secondary flows and turbulence levels to enhance mixing, and form coherent fluid motions in the form of streamwise oriented vortices, and also to provide some heat transfer augmentation by increasing surface areas for convective heat transfer [1]. This is a problem of conjugate heat transfer within a heterogeneous hierarchical structure. It is not easy to optimize this kind of problem since many parameters are required to describe the geometry. Simple equations are the only answer if one wants to find the optimum configuration for these kinds of conjugate heat transfer devices.

2.1. VAT based governing equations

Based on rigorous averaging techniques developed by Whitaker [21,22] who focused on solving linear diffusion problems and by Travkin and Catton [24,26] who focused on solving nonlinear turbulent diffusion problems, the thermal physics and fluid mechanics governing equations in heterogeneous porous media were developed from the Navier-Stokes equation and the thermal energy equations. This is the starting point for studying flow and heat transfer in porous media and also the basis of the present work.

In this section, a model based on VAT is developed to describe transport phenomena in plane fin heat sinks with shielded top, at which a boundary condition of nonslip wall is applied. The air flow is considered to be 'porous flow', in which the term 'porous' is used in a broad sense.

The momentum equation is

$$0 = -\frac{1}{\rho_f}\frac{d\langle \bar{p} \rangle_f}{dx} + f^* \frac{S_w}{\langle m(z) \rangle}\frac{\tilde{\bar{u}}^2}{2} + \frac{\partial}{\partial z}\left(\langle m(z) \rangle (\nu + \nu_t)\frac{\partial \tilde{\bar{u}}}{\partial z} \right) \quad (1)$$

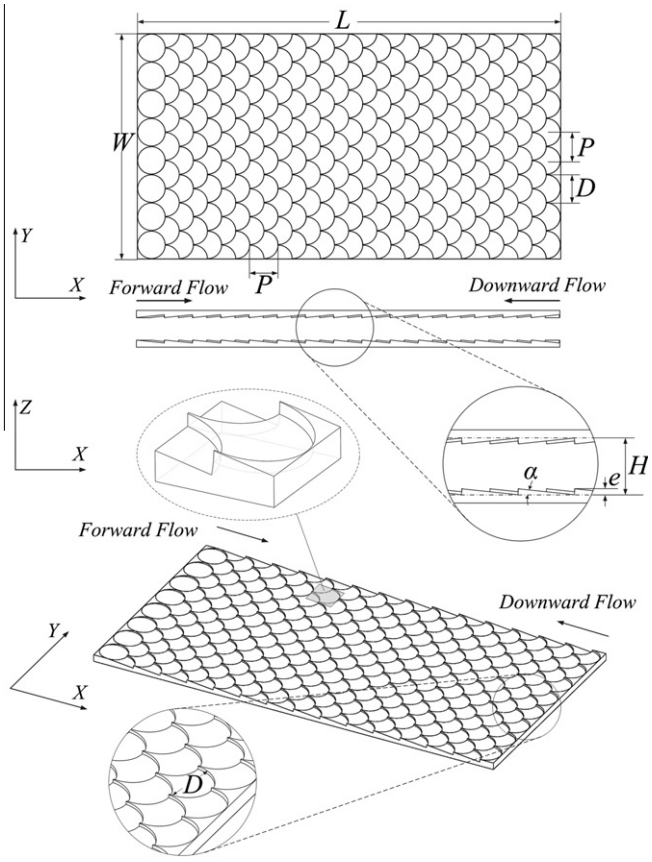

Fig. 1. Geometrical details of scale-roughened surface.

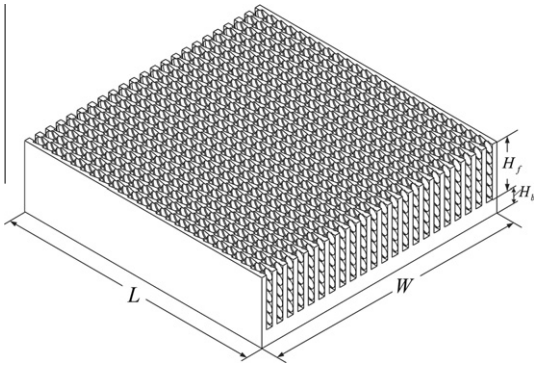

Fig. 2. A plane fin heat sink with scale roughened surfaces.

The energy equation for fluid phase is

$$\rho_f c_{pf}\langle m\rangle\tilde{\tilde{u}}\frac{\partial\tilde{\tilde{T}}_f}{\partial x}=\frac{\partial}{\partial z}\left(\langle m\rangle(k_f+\tilde{k}_t)\frac{\partial\tilde{\tilde{T}}_f}{\partial z}\right)+h^*S_w(\tilde{T}_s-\tilde{\tilde{T}}_f) \tag{2}$$

The energy equation for solid phase is

$$\frac{\partial}{\partial x}\left[(1-\langle m\rangle)k_s\frac{\partial\tilde{T}_s}{\partial x}\right]+\frac{\partial}{\partial z}\left[(1-\langle m\rangle)k_s\frac{\partial\tilde{T}_s}{\partial z}\right]=h^*S_w(\tilde{T}_s-\tilde{\tilde{T}}_f) \tag{3}$$

2.2. Closure terms of the VAT equations

To complete the VAT based model, four closure terms need to be evaluated. It is believed that the only way to achieve substantial gains is to maintain the connection between porous media morphology and the rigorous formulation of mathematical equations for transport.

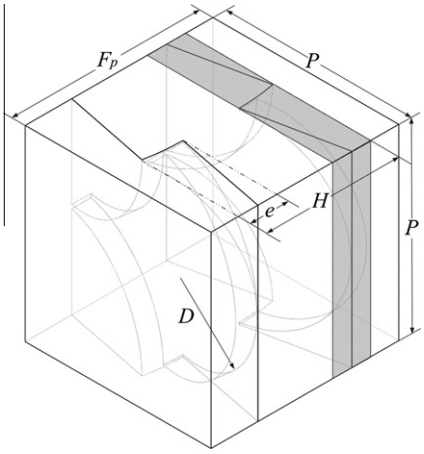

Fig. 3. Representative elementary volume (REV) for a PFHS with scale roughened surfaces.

Two of the closure terms, the averaged porosity and the specific surface area are geometrically defined and it is quite easy to determine them if one selects the REV correctly. The selection for a PFHS with scale roughened surface, see Fig. 3 is seen to repeat in both the cross-stream and flow directions. Therefore, the porosity is

$$\langle m\rangle=1-\frac{\Delta\Omega_s}{\Delta\Omega}=\frac{H-2\kappa e}{F_p} \tag{4}$$

in which, $\Delta\Omega$ is the volume of the REV defined as

$$\Delta\Omega=P^2F_p=D^2F_p \tag{5}$$

$\Delta\Omega_s$ is the volume of the solid part of the REV defined by

$$\Delta\Omega_s=D^2(F_p-H)+2\kappa eD^2 \tag{6}$$

in which κ is the ratio of the solid volume of the scale to the total volume of the $e\times P\times P$ slab, see the shaded part in Fig. 3. It can easily be shown that κ is a constant and $\kappa=\frac{3}{4}-\frac{\pi}{8}$.

The specific surface area, S_w, is defined as

$$S_w=\frac{A_w}{\Delta\Omega}=\frac{2P^2+\pi De}{P^2F_p}=\frac{2D+\pi e}{DF_p} \tag{7}$$

At this point, the VAT based model of scale-roughened PFHS is still not fully closed. The other two closure terms are the local friction factor, f^*, in the momentum equation and the local heat transfer coefficient, h^*, in the VAT energy equations and remain to be evaluated. To evaluate the closure terms, a commercial finite volume method (FVM)-based code, CFX, was used to analyze the convective heat transfer in three-dimensional channels with opposing scale-roughened walls.

3. Numerical method and procedures

3.1. Computational domain and boundary conditions

The local closure values or closure values for fully developed flow and heat transfer are the only kinds of closure values that have physical meaning when describing transport phenomena with VAT based equations. For this reason, attention should be paid to the selection of physical model. The computational domain should be long enough, so that closure can be evaluated over an REV that is not affected by entrance or re-circulation effects near

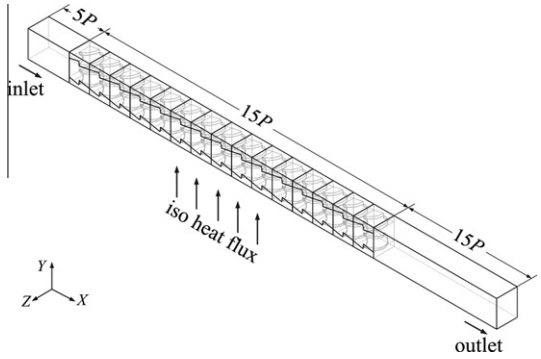

Fig. 4. Computational domain. The length of the extended region was not drawn in scale.

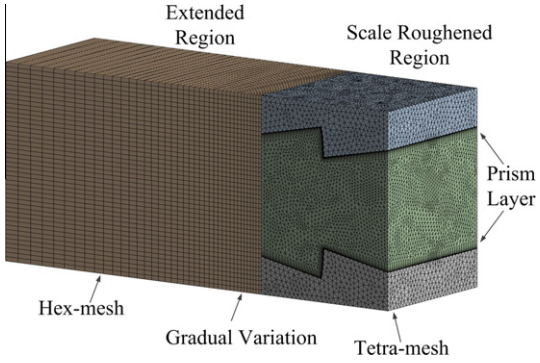

Fig. 5. Example of the grid system. Only part of the whole model is shown.

Table 1
Boundary conditions.

Inlet	u = const, $v = w = 0$, T = const
Outlet	$\frac{\partial u_i}{\partial x} = \frac{\partial T}{\partial x} = 0$
Eight surfaces of the extended region	Symmetric, slip and adiabatic wall
Interface between air and solid	No-slip, no thermal resistance
The bottom of the scale roughened wall	Iso heat flux
The other surfaces	Symmetric

the outlet [36]. A computational domain with fifteen REVs was selected as the computational domain, see Fig. 4.

The air velocity profile at the entrance is not uniform because of the fin thickness. The computational domain is extended upstream a distance of five stream-wise REV lengths so that a uniform velocity distribution can be ensured at the domain inlet. The computational domain is extended downstream 15 times the stream-wise REV length, so that at the outer flow boundary no flow recirculation exits. The boundary conditions applied to the computational domain are tabulated in Table 1.

3.2. Grid system

The grid systems for all the scale-roughened channel models are built by Ansys Meshing. Due to the roughness of the wall, unstructured tetra-mesh is created for the scale-roughened test channel, with prism layers being inserted in the near wall region. In the extended regions, a coarser and structured hex-mesh is adopted to conserve computational resources. A grid system with a gradual variation in and after the scale-roughened test channel is used to avoid the undesirable effect of an abrupt grid width change in the computing region. The grid system for one of the models is shown in Fig. 5.

Grid independence tests were made carefully by recursive refinement and comparison between the numerical simulation results. The above process was repeated until the variation of Nusselt number and friction factor was less than 0.5%, so that the numerical predictions can be regarded as grid-independent. With the turbulence predictions employed, the meshes near the fluid solid interface are fine enough to resolve the flow behavior close to the no-slip wall. For all the simulation cases, y^+ values in the near-wall region are less than 1.

3.3. Mathematical model

The air flow is assumed to be three-dimensional, incompressible, steady state. In the low Reynolds number region, the flow is assumed to be laminar, while for $Re > 2000$, a turbulent model is adopted. Buoyancy and radiation heat transfer effects are not taken into consideration. The three-dimensional governing equations for continuity, momentum and energy are as follows:

(1) Continuity equation

$$\frac{\partial \rho u_i}{\partial x_i} = 0 \tag{8}$$

(2) Momentum equation

$$\rho u_j \frac{\partial u_i}{\partial x_j} = \frac{\partial}{\partial x_j}\left[(\mu + \mu_t)\frac{\partial u_i}{\partial x_j}\right] - \frac{\partial p}{\partial x_i} \tag{9}$$

(3) Energy equation

$$\rho u_j \frac{\partial T}{\partial x_j} = \frac{\partial}{\partial x_j}\left[\left(\frac{\mu}{\mathrm{Pr}} + \frac{\mu_t}{\mathrm{Pr}_t}\right)\frac{\partial T}{\partial x_j}\right] \tag{10}$$

The k–ω based Shear-Stress-Transport (SST) model with automatic wall function treatment is used to predict the turbulent flow and heat transfer through the channel. The SST model blends the robust and accurate formulation of the k–ω model in the near-wall region with the free-stream independence of the k–ε model in the far field. The SST model gives a highly accurate prediction of the onset and the amount of flow separation under adverse pressure gradients by the inclusion of transport effects into the formulation of the eddy-viscosity. This results in a major improvement in terms of flow separation predictions. The superior performance of the SST model has been demonstrated for high accuracy boundary layer simulations in a large number of validation studies.

Menter [37,38] proposed the equations for the SST model as

$$\frac{D(\rho k)}{Dt} = \widetilde{P}_k - \beta^* \rho k \omega + \frac{\partial}{\partial x_j}\left[(\mu + \sigma_k \mu_t)\frac{\partial k}{\partial x_i}\right] \tag{11}$$

$$\frac{D(\rho \omega)}{Dt} = \alpha \rho S^2 - \beta \rho \omega^2 + \frac{\partial}{\partial x_i}\left[(\mu + \sigma_\omega \mu_t)\frac{\partial \omega}{\partial x_i}\right] + 2(1 - F_1)\rho \sigma_{\omega_2}\frac{1}{\omega}\frac{\partial k}{\partial x_i}\frac{\partial \omega}{\partial x_i} \tag{12}$$

where the blending function F_1 is defined by:

$$F_1 = \tanh\left\{\left\{\min\left[\max\left(\frac{\sqrt{k}}{\beta^* \omega y}, \frac{500v}{y^2 \omega}\right), \frac{4\rho \sigma_{\omega_2} k}{CD_{k\omega} y^2}\right]\right\}^4\right\} \tag{13}$$

in which

$$CD_{k\omega} = \max\left(2\rho \sigma_{\omega_2}\frac{1}{\omega}\frac{\partial k}{\partial x_j}\frac{\partial \omega}{\partial x_j}, 10^{-10}\right) \tag{14}$$

The turbulent eddy viscosity is computed from:

$$v_t = \frac{a_1 k}{\max(a_1 \omega, SF_2)} \tag{15}$$

where S is the invariant measure of the strain rate and F_2 is a second blending function defined by

$$F_2 = \tanh\left\{\left[\max\left(2\frac{\sqrt{k}}{\beta^*\omega y}, \frac{500v}{y^2\omega}\right)\right]^2\right\} \tag{16}$$

To prevent the build-up of turbulence in stagnation regions, a production limiter is used in the SST model:

$$P_k = \mu_t \frac{\partial u_i}{\partial x_j}\left(\frac{\partial u_i}{\partial x_j} + \frac{\partial u_j}{\partial x_i}\right) \rightarrow \widetilde{P}_k = \min(P_k, 10 \cdot \beta^* \rho k \omega) \tag{17}$$

Each of the constants is a blend of the corresponding constants of the k–ε and the k–ω model:

$$\varphi = F_1\varphi_1 + (1 - F_1)\varphi_2 \tag{18}$$

The constants for this model take the following values

$$\begin{aligned} &\beta^* = 0.09, \\ &\alpha_1 = 5/9,\ \ \beta_1 = 3/40,\ \ \sigma_{k1} = 0.85,\ \ \sigma_{\omega 1} = 0.5, \\ &\alpha_2 = 0.44,\ \ \beta_2 = 0.0828,\ \ \sigma_{k2} = 1,\ \ \sigma_{\omega 2} = 0.856. \end{aligned} \tag{19}$$

The CFD code solves the Reynolds-averaged Navier–Stokes equations with a high resolution scheme for the advection terms as well as turbulence numerics. The fully coupled momentum and energy equations are solved simultaneously. The RMS type residual for solution convergence criteria is set to be 10^{-5} for the momentum balance and 10^{-6} for the energy equation.

4. Closure evaluation

Closure evaluation described in this section consists of three parts. First, the two different length scales used to evaluate the flow and heat transfer characteristics of the scale-roughened channels are defined. Second, the computational model and the method adopted in current numerical simulations are verified and validated by comparing the CFD results with experimental data. Third, two correlations which serve as closure for the VAT based model are developed based on the simulation results.

4.1. Length scales

Before evaluating the closure terms, it is interesting to note that using a particular length scale leads to a parameter that is very beneficial when evaluating the heat transfer coefficient and friction factor. It was shown by Travkin and Catton [26] that globular media morphologies can be described in terms of S_w, $\langle m\rangle$ and d_p and can generally be considered to be spherical particles with

$$S_w = \frac{6(1 - \langle m\rangle)}{d_p} \tag{20}$$

$$D_h = \frac{2}{3}\frac{\langle m\rangle}{(1 - \langle m\rangle)}d_p \tag{21}$$

This expression has the same dependency on equivalent pore diameter as found for a one diameter capillary morphology leading naturally to

$$S_w = \frac{6(1 - \langle m\rangle)}{d_p} = \frac{6(1 - \langle m\rangle)}{\frac{3}{2}\frac{(1-\langle m\rangle)}{\langle m\rangle}D_h} = \frac{4\langle m\rangle}{D_h} \tag{22}$$

This observation leads to defining a simple "universal" porous media length scale

$$D_h = \frac{4\langle m\rangle}{S_w} \tag{23}$$

that meets the needs of both morphologies: capillary and globular. This was also recognized by Whitaker [22] when he used a very similar (differing by a constant) length scale to correlate heat transfer for a wide variety of morphologies. Zhou et al. [39] also showed that using the 'porous media' length scale is very beneficial in collapsing complex data yielding simple heat transfer and friction factor correlations. For the present scale-roughened channel, D_h is defined as

$$D_h = \frac{4\langle m\rangle}{S_w} = \frac{4D(H - 2\kappa e)}{2D + \pi e} \tag{24}$$

It can be seen that D_h is a function of e, D and H.

The Reynolds number defined using the VAT suggested length scale is

$$Re_{D_h} = \frac{\rho u_m D_h}{\mu} \tag{25}$$

To validate the CFD simulation results, the Reynolds number is defined the same as that used by Chang et al. [14]

$$Re = \frac{\rho u_m d_h}{\mu} \tag{26}$$

in which d_h is the hydraulic diameter defined by

$$d_h = 2 \cdot H \cdot W/(H + W) \tag{27}$$

The averaged Nusselt number in the developed region used for validation is defined as

$$Nu = \frac{qd_h}{k_f(\overline{T_s} - \overline{T_f})} \tag{28}$$

The friction factor for validation is defined as

$$f = \frac{\Delta p}{\frac{1}{2}\rho u_m^2}\frac{d_h}{4L} \tag{29}$$

4.2. Validation and verification

To verify the computational model and the method adopted in numerical simulation, preliminary computations were first conducted for a scale roughened channel which had the same dimensions as the one experimentally tested by Chang et al. [14]. A quarter of the full test section is selected to be the computational domain, see Fig. 6. From the figure we can see that the maximum deviation of the Nusselt number and the friction factor from experiment are 6.3% and 12.1% with the average deviation being around 3.5% and 5.8% respectively. Our predicted results and the

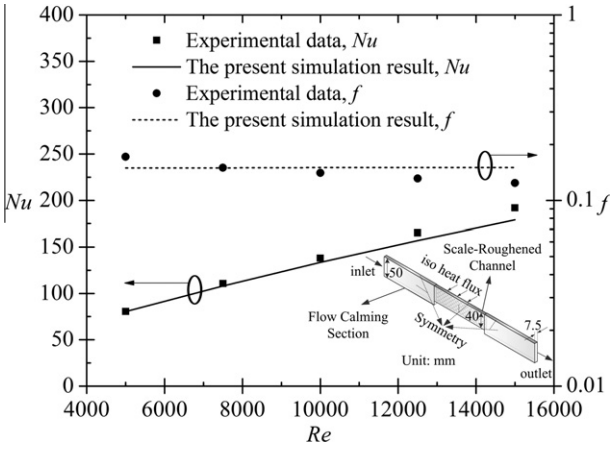

Fig. 6. Validation of the present CFD simulation by comparing with experimental data by Chang et al. [14].

experimental data agree very well, thereby showing the reliability of the physical model and the adopted numerical method.

4.3. Mechanism of heat transfer enhancement by Scales

To have a qualitative view into the flow behavior, Fig. 7 provides insight into the local distributions of the streamlines on three cross-sections in the y–z planes normal to the flow direction at Re = 10,000. The three planes are located at the inlet, the center plane and outlet of the eleventh REV, showing how the streamlines develop when the fluid flows through one cycle of scale-roughened channel. It is found that when the flow starts entering the REV, some cone-shaped streamlines are formed above the scales. After that the flow starts spinning in the span-wise direction. As the fluid flows farther downward, the spinning becomes stronger. The strong spinning of the flow breaks the near wall boundary layers continuously and enhances the bulk flow mixing. It is easy for the readers to turn the plane streamlines into 3D footage in mind and imagine how the flow is marching in a spiral pattern. This explains why the heat transfer is augmented by the scale-roughened surface.

4.4. Closure

Travkin and Catton [26] rigorously derive the closure terms for VAT based model from the lower scale governing equations. The closure term in the VAT momentum equation, f^*, has the form

$$f^* = 2\frac{\int_{\partial S_w}\tilde{p}\cdot d\vec{s}}{\rho_f\tilde{\bar{u}}^2A_{wp}}\frac{S_{wp}}{S_w} + 2\frac{\int_{\partial S_w}\tau_{wL}\cdot d\vec{s}}{\rho_f\tilde{\bar{u}}^2A_w} + 2\frac{\int_{\partial S_w}\tau_{wT}\cdot d\vec{s}}{\rho_f\tilde{\bar{u}}^2A_w} - \frac{\frac{\partial}{\partial x_j}\langle\hat{\tilde{u}}_i\hat{\tilde{u}}_j\rangle_f}{\frac{1}{2}\rho\tilde{\bar{u}}^2} + \frac{\frac{\partial}{\partial x_j}\left(\langle\tilde{v}_T\frac{\partial\tilde{u}_i}{\partial x_j}\rangle_f\right)}{\frac{1}{2}\rho\tilde{\bar{u}}^2} \tag{30}$$

The first three terms are form drag, and laminar and turbulent contributions to skin friction, respectively. The fourth term represents the spatial flow oscillations, which are a function of porous media morphology and tell one how flow deviates from some mean value over the REV. The fifth term represents flow oscillations that are due to Reynolds stresses and are a function of porous media morphology and its time averaged flow oscillations.

The closure terms in the VAT energy equation, h^*, can be defined in various ways and in general will depend on how many of the integrals appearing in the VAT equation one uses and lumps into a single transport coefficient, see Travkin and Catton [26]. The nature of the equation shows that the energy transferred from the surface is integrated over an area and then divided by the chosen REV volume; therefore, the heat transfer coefficient is defined in terms of porous media morphology, usually described by specific surface and porosity.

The complete form of the closure term h^* is

$$h^* = \frac{\frac{1}{\Delta\Omega}\int_{\partial S_w}(k_f+k_t)\nabla T_f\cdot d\vec{s}}{S_w(\widetilde{T}_s-\widetilde{T}_f)} - \frac{\rho_f c_{pf}\nabla\cdot(\langle m\rangle\widetilde{\hat{u}_f\hat{T}_f})}{S_w(\widetilde{T}_s-\widetilde{T}_f)} + \frac{\nabla\cdot\left(\frac{k_f}{\Delta\Omega}\int_{\partial S_w}T_f d\vec{s}\right)}{S_w(\widetilde{T}_s-\widetilde{T}_f)} \tag{31}$$

In most engineered devices, the geometry is regular and a well-chosen REV will lead to only the first term being needed. The second term is identically zero for regular repeating geometries and the third is Biot number dependent. However, when in doubt, one should use the complete form given by Eq. (31).

After solving the three-dimensional governing equations (8)–(10) with appropriate boundary conditions, the closure for the VAT based momentum equation and energy equation is obtained by integrating Eqs. (30) and (31) over the selected REV to compute the friction factor and heat transfer coefficient.

To make the correlations applicable to relatively wide range of dimensions of scale roughened channels, 20 different sets of design dimensions, see Table 2, were simulated at different Reynolds numbers, ranging from 500 to 3×10^4. It should be noted that, for all the design points, the scale pitch is equal to the diameter of the scale, which is the only sensible way to lay out the disc shaped scales. The ratio of the scale height to the scale diameter, e/D, or the angle of attack, $\alpha = \arcsin(e/D)$, defines the shape of the scales. The ratio of the channel height to the scale diameter, H/D, specifies the shape of the channel. Therefore, e/D and H/D could specify the shape of the REV. The REVs, which have the same e/D and H/D but different scale diameters, are dynamically similar, and they are governed by the same physical laws and associated equations, which produce exactly the same solution in terms of dimensionless variables, such as Nu and f, at the same Re. Therefore, e/D and H/D are selected to be the design parameters. However, since D_h is a function of e, D and H, and D_h is the chosen length scale, the heat transfer and friction closure relationships were correlated in terms of e/D_h and H/D_h, using a multiple regression technique.

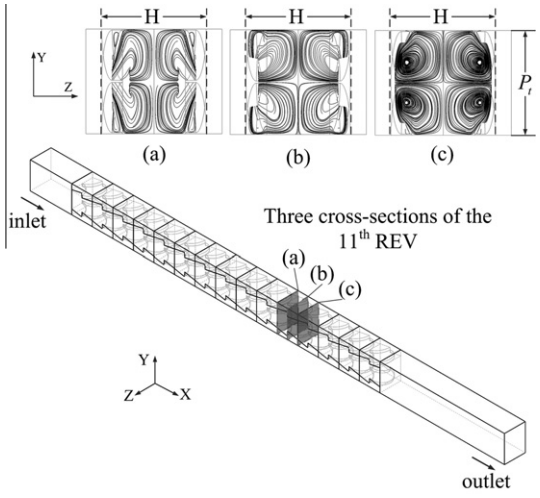

Fig. 7. Streamlines on the planes normal to flow direction, Re = 10,000.

Table 2
Dimensions of the numerically tested models.

Model	e/D	H/D
1	0.05	0.75
2	0.05	1.25
3	0.05	1.75
4	0.05	2.25
5	0.1	0.75
6	0.1	1.25
7	0.1	1.75
8	0.1	2.25
9	0.15	0.75
10	0.15	1.25
11	0.15	1.75
12	0.15	2.25
13	0.2	0.75
14	0.2	1.25
15	0.2	1.75
16	0.2	2.25
17	0.25	0.75
18	0.25	1.25
19	0.25	1.75
20	0.25	2.25

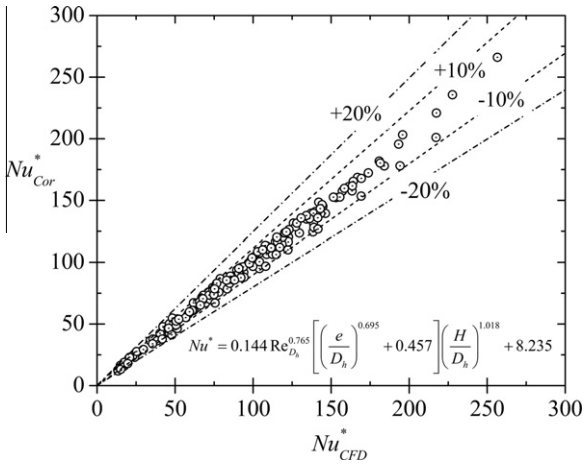

Fig. 8. Deviation of the proposed Nusselt number correlation.

The resulting Nusselt number correlation is

$$Nu^* = \frac{h^* D_h}{\lambda_f} = 0.144\,Re_{D_h}^{0.765}\left[\left(\frac{e}{D_h}\right)^{0.695} + 0.457\right]\left(\frac{H}{D_h}\right)^{1.018} + 8.235 \quad (32)$$

The resulting friction factor is in the form

$$f^* = \frac{94.53}{Re_{D_h}} + 0.0019\,Re_{D_h}^{0.217} + 3.544\left(\frac{e}{D_h}\right)^{1.465}\left(\frac{H}{D_h}\right)^{0.0232} \quad (33)$$

Figs. 8 and 9 show the comparison between the numerical simulation results and the results predicted by the proposed correlations. The proposed heat transfer correlation, Eq. (32), can describe all the simulation results within a deviation of 15% and 98.2% of them within 10%. The correlation of friction factor, Eq. (33), can predict 90.5% of data within a deviation of 10% and all of them within a deviation of 20%. The correlations of Nusselt number and friction factor have an average deviation of 3.2% and 5.4% respectively.

It should be noted that the present correlations are not only applicable to scale-roughened channels but also converge to smooth channels when $e = 0$. From the definition of D_h, Eq. (24), it is known that $D_h = 2H$ as e becomes zero and the proposed correlations converged to

$$Nu^* = 0.0325\,Re_{D_h}^{0.765} + 8.235 \quad (34)$$

and

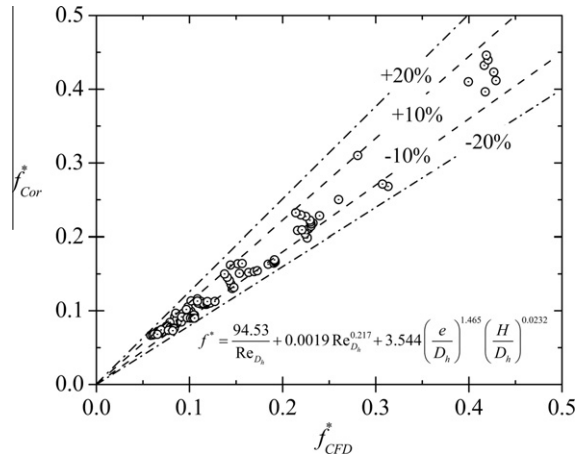

Fig. 9. Deviation of the proposed friction factor correlation.

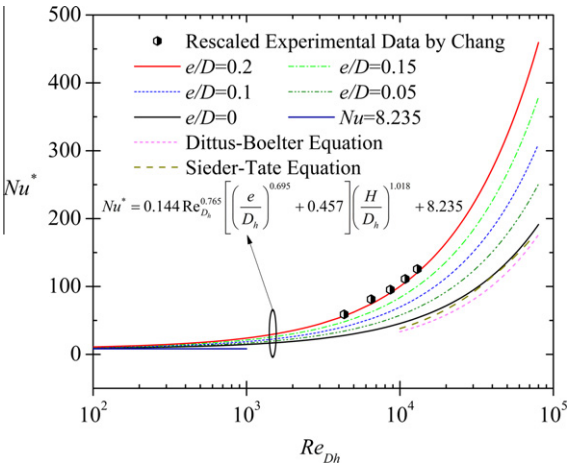

Fig. 10. Comparison of the present *Nu* correlation and rescaled experimental data, and some well-known correlations for smooth channel.

$$f^* = \frac{94.53}{Re_{D_h}} + 0.0019\,Re_{D_h}^{0.217} \quad (35)$$

To validate the predictive capability of the present correlations, the results predicted by Eqs. (32) and (33) for different e/D are compared with the rescaled experimental data by Chang et al. [14] as shown in Figs. 10 and 11, see Zhou et al. [39] on how to rescale available experimental data using the VAT suggested length scale. Both Figs. 10 and 11 show that the rescaled experimental data by Chang et al. [14] and the proposed correlations agree very well.

To further check whether our correlations converged to smooth channel when $e = 0$, a few well known correlations for smooth channels are brought into the comparison. It is shown in Fig. 10 that the converged *Nu* correlation, Eq. (34), for smooth parallel plate channel can predict the Nusselt number with an average deviation of 4.1% from the correlation proposed by Sieder and Tate [40] and around 13% above Dittus–Boelter equation [41] for turbulent flow. Also, when Reynolds is decreased, the Nusselt number converges to the analytical solution for laminar flow through parallel plate ducts with uniform heat flux at two walls, which is $Nu = 8.235$. From Fig. 11, it is seen that the converged friction factor correlation, Eq. (35), almost coincides with the analytical solution for laminar flow through parallel plate ducts, which is $f = 96/Re_{D_h}$, and the correlation by Beavers et al. [42] for turbulent flow.

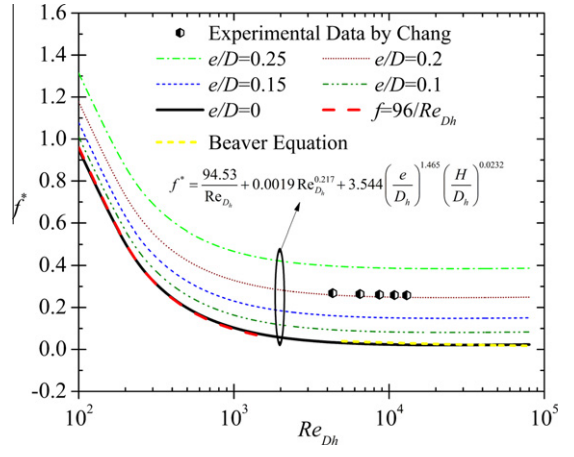

Fig. 11. Comparison of the present *f* correlation and rescaled experimental data, and some well-known correlations for smooth channel.

It should be noted that the correlations proposed in the present work are not necessarily the most accurate, however, they have wide application, are easy to use, and are quite satisfactory for most design calculations [22]. Also, for optimization, extreme accuracy is not vital because variation in the parameter being optimized can be as much as an order of magnitude.

At this point, the VAT based model of PFHS with scale roughened surfaces is fully closed. With the closure correlations, the governing equation set is relatively simple and can be solved discretely in seconds. With the help of a statistical tool for Design of Experiments (DOE) or Genetic Algorithm (GA), a scale roughened PFHS could be designed and optimized in an hour, instead of days of CFD or experimental work. How to design and optimize a scale roughened PFHS based on VAT will be presented in a future paper.

5. Concluding remarks

Volume averaging theory is little more than a judicious application of Green's and Stokes' theorems to carry out the integration needed to average the point-wise conservation equations in a rigorous way. By treating the closure part of the problem carefully, the result remains rigorous in spite of its simplicity. Many everyday engineered devices are hierarchical and heterogeneous and can be effectively treated by application of VAT. It is an approach that can be applied to many different types of transport phenomena, see Travkin and Catton [26].

The present paper describes an effort to develop a VAT based hierarchical model for a plane fin heat sink with scale roughened surfaces and obtain the closure for the model by CFD code. A length of 15 REVs was selected to be the computational domain. The rigorously derived closure terms represented as heat transfer coefficient and friction factor were evaluated over the carefully selected REV. Correlations of friction factor and Nusselt number were established based on the simulation results.

With closure in terms of the friction factor and the heat transfer coefficient, the problem is closed and the porous media governing equations derived from VAT are

$$\widetilde{M}(\langle m\rangle, S_w, f^*) \tag{36}$$

$$\widetilde{T}_s(\langle m\rangle, S_w, h^*) \tag{37}$$

$$\widetilde{T}_f(\langle m\rangle, S_w, h^*) \tag{38}$$

where $\widetilde{M}$ stands for averaged momentum equation variables, $\widetilde{T}_s$ and $\widetilde{T}_f$ stand for averaged energy equation variables for solid and fluid phase. The macro scale equations are functions only of porous media morphology, represented by porosity and specific surface area, and its closure.

Acknowledgment

The support of a DARPA initiated grant within the MACE program, Grant No. W31P4Q-09-1-0005, is gratefully acknowledged. The views, opinions, and/or findings contained in this article are those of the author and should not be interpreted as representing the official views or policies, either expressed or implied, of the Defense Advanced Research Projects Agency or the Department of Defense.

References

[1] P.M. Ligrani, M.M. Oliveira, T. Blaskovich, Comparison of heat transfer augmentation techniques, AIAA J. 41 (3) (2003) 337–362.
[2] M.E. Taslim, T. Li, D.M. Kercher, Experimental heat transfer and friction in channels roughened with angled, V-shaped, and discrete ribs on two opposite walls, J. Turbomach. Trans. ASME 118 (1) (1996) 20–28.
[3] J.C. Han, Y.M. Zhang, C.P. Lee, Augmented heat transfer in square channels with parallel, crossed, and V-shaped angled ribs, J. Heat Transfer 113 (3) (1991) 590–596.
[4] X. Gao, B. Sunden, Heat transfer and pressure drop measurements in rib-roughened rectangular ducts, Exp. Therm. Fluid Sci. 24 (1–2) (2001) 25–34.
[5] J.S. Park, J.C. Han, Y. Huang, S. Ou, R.J. Boyle, Heat transfer performance comparisons of five different rectangular channels with parallel angled ribs, Int. J. Heat Mass Transf. 35 (11) (1992) 2891–2903.
[6] H.H. Cho, S.J. Wu, H.J. Kwon, Local heat/mass transfer measurements in a rectangular duct with discrete ribs, J. Turbomach. 122 (3) (2000) 579–586.
[7] K. Park, D.-H. Choi, K.-S. Lee, Optimum design of plate heat exchanger with staggered pin arrays, Numerical Heat Transfer, Part A: Applications: An International Journal of Computation and Methodology 45 (4) (2004) 347–361.
[8] W.A. Khan, J.R. Culham, M.M. Yovanovich, The role of fin geometry in heat sink performance, J. Electron. Packag. 128 (4) (2006) 324–330.
[9] F. Zhou, I. Catton, Numerical evaluation of flow and heat transfer in plate-pin fin heat sinks with various pin cross-sections, Numerical Heat Transfer, Part A: Applications 60 (2) (2011) 107–128.
[10] G.I. Mahmood, M.L. Hill, D.L. Nelson, P.M. Ligrani, H.K. Moon, B. Glezer, Local heat transfer and flow structure on and above a dimpled surface in a channel, J. Turbomach. 123 (1) (2001) 115–123.
[11] G.I. Mahmood, P.M. Ligrani, Heat transfer in a dimpled channel: combined influences of aspect ratio, temperature ratio, Reynolds number, and flow structure, Int. J. Heat Mass Transf. 45 (10) (2002) 2011–2020.
[12] N.K. Burgess, P.M. Ligrani, Effects of dimple depth on channel Nusselt numbers and friction factors, J. Heat Transfer 127 (8) (2005) 839–847.
[13] G.I. Mahmood, M.Z. Sabbagh, P.M. Ligrani, Heat transfer in a channel with dimples and protrusions on opposite walls, J. Thermophys. Heat Transfer 15 (3) (2001) 275–283.
[14] S.W. Chang, T.-M. Liou, M.H. Lu, Heat transfer of rectangular narrow channel with two opposite scale-roughened walls, Int. J. Heat Mass Transf. 48 (19–20) (2005) 3921–3931.
[15] S.W. Chang, T.M. Liou, K.F. Chiang, G.F. Hong, Heat transfer and pressure drop in rectangular channel with compound roughness of V-shaped ribs and deepened scales, Int. J. Heat Mass Transf. 51 (3–4) (2008) 457–468.
[16] S.W. Chang, T.L. Yang, T.-M. Liou, H.G. Fang, Heat transfer in rotating scale-roughened trapezoidal duct at high rotation numbers, Appl. Therm. Eng. 29 (8–9) (2009) 1682–1693.
[17] S.W. Chang, T.L. Yang, T.-M. Liou, G.F. Hong, Heat transfer of rotating rectangular duct with compound scaled roughness and V-ribs at high rotation numbers, Int. J. Therm. Sci. 48 (1) (2009) 174–187.
[18] S.W. Chang, A.W. Lees, Endwall heat transfer and pressure drop in scale-roughened pin-fin channels, Int. J. Therm. Sci. 49 (4) (2010) 702–713.
[19] T.B. Anderson, R. Jackson, Fluid mechanical description of fluidized beds, Equations of Motion, Industrial & Engineering Chemistry Fundamentals 6 (4) (1967) 527–539.
[20] J.C. Slattery, Flow of viscoelastic fluids through porous media, AIChE J. 13 (6) (1967) 1066–1071.
[21] S. Whitaker, Diffusion and dispersion in porous media, AIChE J. 13 (3) (1967) 420–427.
[22] S. Whitaker, Forced convection heat transfer correlations for flow in pipes, past flat plates, single cylinders, single spheres, and for flow in packed beds and tube bundles, AIChE J. 18 (2) (1972) 361–371.
[23] V. Travkin, I. Catton, A two-temperature model for turbulent flow and heat transfer in a porous layer, J. Fluids Eng. 117 (1) (1995) 181–188.
[24] V.S. Travkin, I. Catton, Porous media transport descriptions – non-local, linear and non-linear against effective thermal/fluid properties, Adv. Colloid Interface Sci. 76–77 (1998) 389–443.
[25] V.S. Travkin, I. Catton, Turbulent flow and heat transfer modeling in a flat channel with regular highly rough walls, Int. J. Fluid Mech. Res. 26 (2) (1999) 159–199.
[26] V.S. Travkin, I. Catton, Transport phenomena in heterogeneous media based on volume averaging theory, Adv. Heat Transfer 34 (2001) 1–144.
[27] T. Masuoka, Y. Takatsu, Turbulence model for flow through porous media, Int. J. Heat Mass Transf. 39 (13) (1996) 2803–2809.
[28] B.V. Antohe, J.L. Lage, A general two-equation macroscopic turbulence model for incompressible flow in porous media, Int. J. Heat Mass Transf. 40 (13) (1997) 3013–3024.
[29] A. Nakayama, F. Kuwahara, A macroscopic turbulence model for flow in a porous medium, J. Fluids Eng. 121 (2) (1999) 427–433.
[30] M.H.J. Pedras, M.J.S. de Lemos, Macroscopic turbulence modeling for incompressible flow through undeformable porous media, Int. J. Heat Mass Transf. 44 (6) (2001) 1081–1093.
[31] A. Horvat, I. Catton, Numerical technique for modeling conjugate heat transfer in an electronic device heat sink, Int. J. Heat Mass Transf. 46 (12) (2003) 2155–2168.
[32] A. Horvat, I. Catton, Application of Galerkin method to conjugate heat transfer calculation, Numerical Heat Transfer, Part B: Fundamentals: An International Journal of Computation and Methodology 44 (6) (2003) 509–531.
[33] A. Horvat, B. Mavko, Hierarchic modeling of heat transfer processes in heat exchangers, Int. J. Heat Mass Transf. 48 (2) (2005) 361–371.
[34] A. Horvat, B. Mavko, Calculation of conjugate heat transfer problem with volumetric heat generation using the Galerkin method, Appl. Math. Model. 29 (5) (2005) 477–495.
[35] A. Vadnjal, Modeling of a Heat Sink and High Heat Flux Vapor Chamber, Ph.D. Thesis, University of California Los Angeles, Los Angeles, 2009.

[36] F. Zhou, N.E. Hansen, D.J. Geb, I. Catton, Determination of the number of tube rows to obtain closure for volume averaging theory based model of fin-and-tube heat exchangers, J. Heat Transfer 133 (12) (2011) 121801.
[37] F.R. Menter, Two-equation eddy-viscosity turbulence models for engineering applications, AIAA J. 32 (8) (1994) 1598–1605.
[38] F.R. Menter, M. Kuntz, R. Langtry, Ten years of industrial experience with the SST turbulence model, Turbul. Heat Mass Transfer 4 (2003) 625–632.
[39] F. Zhou, N.E. Hansen, D.J. Geb, I. Catton, Obtaining closure for fin-and-tube heat exchanger modeling based on volume averaging theory (VAT), J. Heat Transfer 133 (11) (2011) 111802.
[40] E.N. Sieder, G.E. Tate, Heat transfer and pressure drop of liquids in tubes, Ind. Eng. Chem. 28 (1936) 1429–1435.
[41] K.E. Gungor, R.H.S. Winterton, A general correlation for flow boiling in tubes and annuli, Int. J. Heat Mass Transf. 29 (3) (1986) 351–358.
[42] G.S. Beavers, E.M. Sparrow, J.R. Lloyd, Low Reynolds number turbulent flow in large aspect ratio rectangular ducts, Trans. ASME, D: J. Basic Eng. 93 (2) (1971). 296-299299.